ULTRASONIC NDT OF IN-PLANE STIFFNESS ANISOTROPY IN METALS AND COMPOSITES

Igor SOLODOV, Daniel DÖRING, Martin RHEINFURTH, and Gerd BUSSE
INSTITUTE OF POLYMER TECHNOLOGY, DEPARTMENT OF NONDESTRUCTIVE TESTING (IKT-ZFP), UNIVERSITY OF STUTTGART,
Pfaffenwaldring 32, 70569 Stuttgart, Germany

1. Introduction

An evident elastic anisotropy is an inherent background for anomalous physical properties and a wide range of applications for the majority of newly developing engineering materials (polymers, composites, ceramics, nano-structures, etc.). As a result, their mechanical performance strongly depends on the orientation of the loads applied and therefore requires detailed information on material stiffness anisotropy. The ultrasonic measurement of stiffness anisotropy is a time consuming procedure which requires cutting material in pieces and testing a number of specimens of various orientations. Mechanical performance of plate-like materials and components, typical for automotive and aviation industries, depends mainly on the in-plane anisotropy of stiffness.

In this paper, two new ultrasonic approaches to NDT of in-plane elastic anisotropy have been developed and applied to various materials including long- and short-fibre reinforced polymer composites as well as metal components. The first approach is based on measurements of shear wave amplitude and phase as functions of its polarization angle. Similar to optics, these waves manifest birefringence due to asymmetry of the in-plane stiffness that results in elliptical particle motion in the material. The parameters of the elliptical motion caused by the birefringence reveal an asymmetry of the in-plane stiffness induced by the lay-up or reinforcement pattern. Such measurements over a specimen area enable evaluation of both homogeneity and local degree of fibre orientation in sheet-like composite materials and the reinforcement induced by plastic deformation in metallic plates.

The other approach uses mode conversion of air-coupled ultrasound to flexural plate waves for remote NDT of the in-plane stiffness anisotropy. The two important features of the flexural wave in-plane anisotropy were experimentally found in laminate materials: it is shown to be both depth-resolved and frequency dependent. The depth-resolution comes from a specific character of material deformation induced by the flexural wave. The bending stiffness which determines the wave velocity is sensitive to the ply lay-up with dominating contribution of the outer plies of the multi-ply composite laminate. This has been confirmed experimentally by revealing substantial in-plane anisotropy of the flexural wave velocity in the specimens with quasi-isotropic lay-ups.

The dynamic elasticity of a plate-like component (even if deemed as made of homogeneous and non-dissipative material) should be regarded as a function of frequency because it depends on the relation between the thickness of the specimen and the wavelength of the elastic response. For low-frequency (axial) loads, the material deformation is due to uniaxial stress and changes for uniaxial strain at higher frequencies. In strongly anisotropic materials, such a transition will be different for various azimuth directions, so that the velocity in-plane anisotropy pattern will depend on frequency. The experimental study is implemented in a frequency range which is wide enough to trace the change of anisotropy in its transition between the two above mentioned regimes and an evident frequency dependence of plate wave velocity anisotropy is observed.

2. Ultrasonic birefringence for NDT of stiffness anisotropy

2.1. Theoretical background

The reinforced materials (e.g. fibre composites) manifest different anisotropic configurations depending on the material structure and composition. The uni- or bidirectional ($0^0/90^0$; $+45^0/-45^0$; etc.) in-plane reinforcements (Fig. 1) induce three orthogonal 2-fold axes of symmetry and display an orthotropic anisotropy. Such anisotropy remains valid as long as both in-plane reinforcement directions (the x- and y-axes, Fig. 1) are not identical.

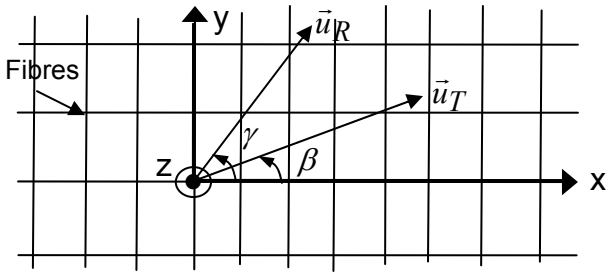

Fig. 1. Coordinate system in [0^0-90^0] reinforced composite material.

For an arbitrary symmetry, characteristics of acoustic wave propagation are obtained from the Christoffel equation [1]:

$$(c_{ijkl} n_j n_l - \rho v^2 \delta_{ik}) u_k = 0\,, \quad (1)$$

where c_{ijkl} are elastic moduli, $n_{j,l}$ are the components of a unit vector in the direction of wave propagation; δ_{ik} is the Kronecker symbol; ρ is the density of the material; v is the acoustic wave velocity; and u_k are the displacement vector components. A non-trivial solution of (1) requires that:

$$\left| \; c_{ijkl} n_j n_l - \rho v^2 \delta_{ik} \; \right| = 0\,, \quad (2)$$

which determines the velocities v_m (m = 1, 2, 3) for a given direction of propagation.

Since composite and metallic materials are often produced in a sheet-like geometry, the wave propagation direction is limited by the z-axis and hence n_3=1; $n_{1,2}$=0. By substituting these values in (1) for the matrix of elastic moduli for the orthotropic symmetry [1] we obtain:

$$(c_{55} - \rho v^2) u_1 = 0\,; \;\; (c_{44} - \rho v^2) u_2 = 0 \;\; ; \; (c_{33} - \rho v^2) u_3 = 0\,. \quad (3)$$

The first two relations in (3) show that velocities for the x- and y-components of an in-plane polarized shear wave are different: $v_1 = \sqrt{c_{55}/\rho}$; $v_2 = \sqrt{c_{44}/\rho}$. The values of the elastic moduli are proportional to the number of fibres in the corresponding direction: $c_{44} > c_{55}$ in the coordinate system Fig. 1, so that the y-axis is a "fast" polarization direction.

Therefore, a linearly polarized shear wave in the material is decomposed into two shear waves propagating with different velocities:

$$\vec{u}_T(z,t) = U_{T_x} \vec{e}_x \sin(\omega t - k_1 z) + U_{T_y} \vec{e}_y \sin(\omega t - k_2 z)\,, \quad (4)$$

where k_1 and k_2 are the wave numbers for the shear waves polarized along the x- and y-axes, respectively; $\vec{e}_x, \vec{e}_y$ are the unit vectors along the corresponding axes. The wave amplitudes in (4) depend on the orientation of the transmitting shear wave transducer: $U_{T_x} = U_T \cos\beta$; $U_{T_y} = U_T \sin\beta$, where β is the angle of the transmitter polarization (Fig. 1) and U_T is the amplitude of its displacement.

Since k_1 and k_2 are different (ultrasonic birefringence), after traversing a plate of the thickness d, the particle displacement acquires (in a general case) an elliptical polarization:

$$\vec{u}_T(d,t) = (U_T \cos\beta)\vec{e}_x \sin\omega t + (U_T \sin\beta)\vec{e}_y \sin(\omega t + \Delta\varphi), \quad (5)$$

where the phase shift is: $$\Delta\varphi = d(k_1 - k_2). \quad (6)$$

If a similar linearly polarized shear wave transducer is used to probe the emerging polarization pattern, the amplitude (V_0) and phase (ψ) of its output signal $V = V_0 \sin(\omega t + \psi)$ are found from (5) [2]:

$$V_0 = U_T \sqrt{\cos^2\beta\cos^2\gamma + \sin^2\beta\sin^2\gamma + 2\sin\beta\cos\beta\sin\gamma\cos\gamma\cos\Delta\varphi} \quad (7)$$

$$\psi = tg^{-1}\left(\frac{\sin\beta\sin\gamma\sin\Delta\varphi}{\cos\beta\cos\gamma + \sin\beta\sin\gamma\cos\Delta\varphi}\right), \quad (8)$$

where γ is the angle between the receiver polarization direction ($\vec{u}_R$, Fig. 1) and the x-axis.

The results of the calculations of output amplitude and phase from (7) and (8) for different in-plane reinforcements are shown in Fig. 2. A high sensitivity of both the output amplitude and phase patterns to variation in the strength of birefringence $\Delta\varphi$, can be applied for NDT of the in-plane asymmetry of reinforcement.

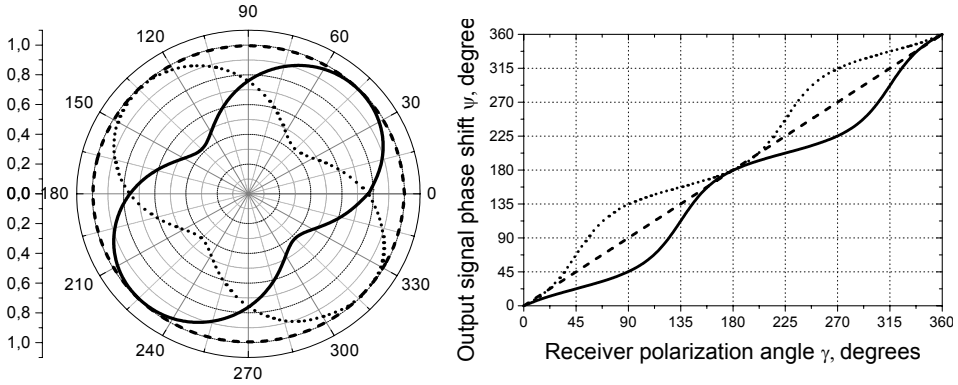

Fig. 2. Output amplitude (left) and phase (right) as functions of receiver polarization angle. Calculations are for $\Delta\varphi$ =45^0 (solid lines); 90^0 (dashed lines); 135^0 (dotted lines) and β =45^0.

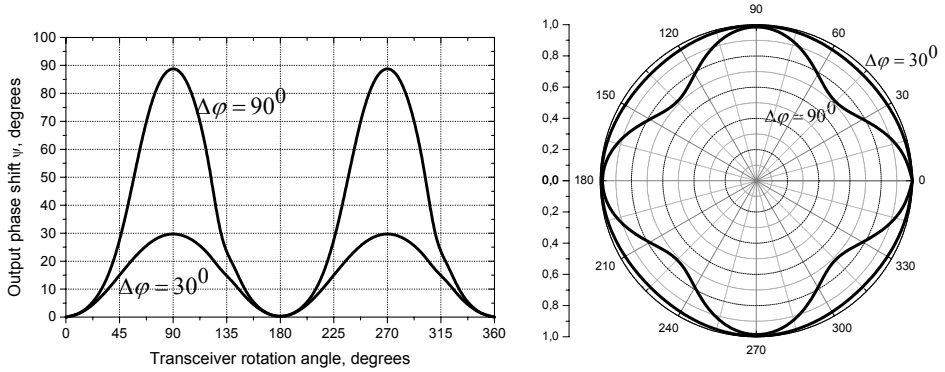

Fig. 3. Output amplitude (right) and phase (left) as functions of receiver polarization angle in reflection mode.

A particular case of $\gamma = \beta$ corresponds to a single transducer measurement (reflection mode). In this case, the output amplitude changes oscillates as $\Delta\varphi$ changes (Fig. 3, right) while the maximum phase variation (see (8)) $\Delta\psi = \Delta\varphi$ (Fig. 3, left), i.e. directly evaluates the asymmetry of reinforcement. The sign of $\Delta\psi$ indicates the sign of the in-plane velocity variation: positive $\Delta\psi$ implies negative temporal shift of the output signal i.e. increase in

velocity and vice versa. The reflection mode is thus well suited for a rapid non-destructive evaluation of a "fast" polarization direction which indicates the fibre orientation.

2. 2. Experimental results: NDT of fibre orientation in composites

The birefringence experiments include shear wave generation/detection followed by the amplitude/phase (delay) measurements of the output signal and can be readily implemented using standard ultrasonic NDT equipment. In our experiments, the Krautkrämer ultrasonic flaw detector (USIP 12) was used for excitation/reception of (2.5 – 4) MHz shear wave pulses generated by piezo-ceramic transducers (K4KY, central frequency 4 MHz). The transducers were attached to the specimens through a layer of viscous ultrasonic coupler; the wave polarization was varied by manual rotation of the transducers. Such a simple setup is sufficient for mapping the predominant reinforcement (fibre) orientation in the reflection mode by monitoring the minimum delay time of the output burst as a function of polarization angle γ ("fast" polarization direction).

For extensive amplitude/phase measurements in the transmission mode (section 3.1), the Ritec 5000 SNAP system was found to be suitable. In this case, 30Vp/p 10-cycle tone bursts were used for excitation of 2.75 MHz-shear waves. After a heterodyne receiver and A/D converter both the amplitude and phase of the output signal are measured automatically via the build-in software.

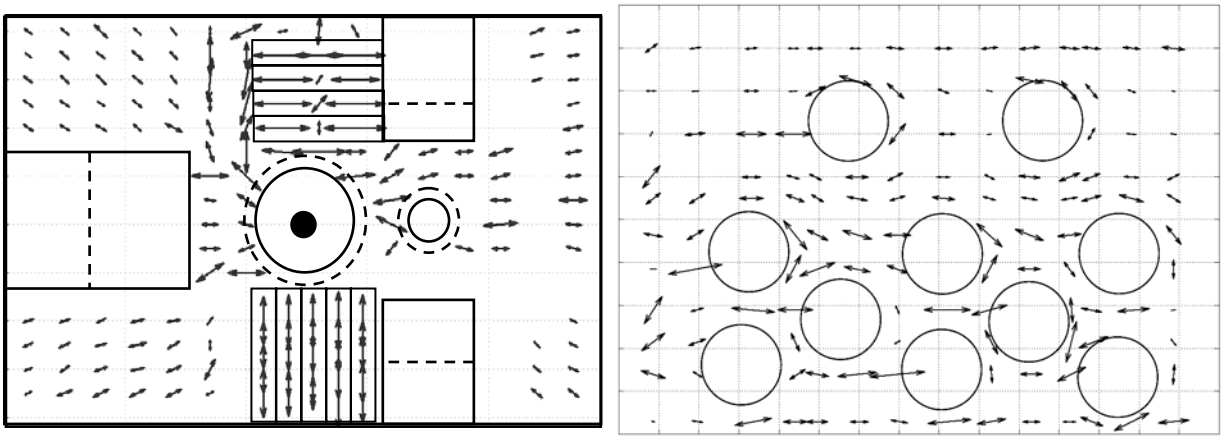

Fig. 4. Mapping of fibre orientation in injection moulding polymer components.

The examples of mapping of short glass fibre orientation in polymer industrial components produced by injection moulding are shown in Fig. 4. The "fast" polarization directions are indicated by arrows; the length of the arrows is proportional to the local degree of reinforcement ($\Delta\varphi$). The specimen in Fig. 4, right is a large (300x200x4 mm) polyurethane plate with the holes formed by circular barriers in the mould. The arrow pattern measured is in a good agreement with expected streamlines in the mould (polymer flow from right to left). Some additional reinforcement observed around the holes is evidently due to accumulation of fibres in the vicinity of the barriers.

The polypropylene specimen in Fig. 4, left has a complex 3D-shape with a series of horizontal and vertical stripes separated by narrow slots. An overall radial arrow pattern is due to a central position of a polymer flow inlet. A drastic enhancement of the fibre alignment is observed in the areas of strips and caused by regularization of the flow around the barriers.

2. 3. NDT of work hardening and friction stir welds in metals

Similar to the fibre reinforcement, material strengthening by plastic deformation can be accompanied by the in-plane anisotropy of stiffness and cause shear wave birefringence. The

measurements of orientation and the degree of reinforcement enable to monitor the efficiency of work hardening.

The case studies of such measurements are given in Fig. 5 for two kinds of cold working produced by rolling (upper row) and shot peening (lower row) in two specimens of Ti- and Ni-base alloys. For each specimen, the low (areas 1 and 3) and high (areas 2 and 4) intensities of surface treatment were applied.

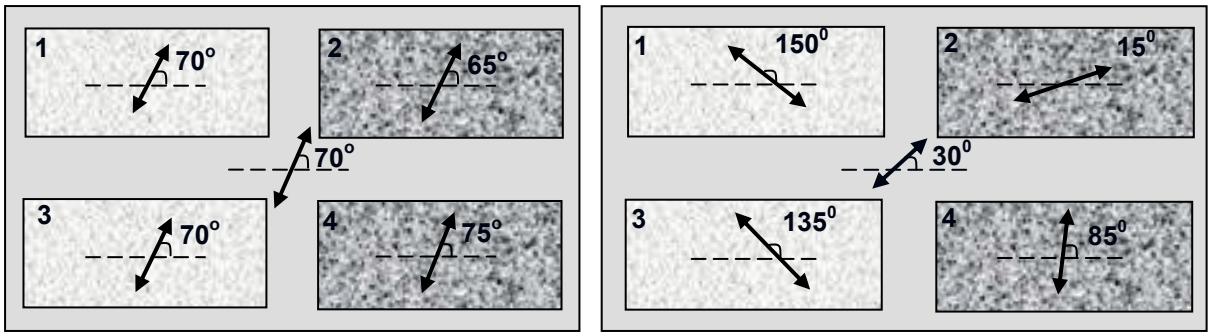

Fig. 5. Orientation of reinforcement produced by rolling (upper row) and shot peening (lower row) in Ti-base (left) and Ni-base (right) alloys.

According to Fig. 5, left, the reinforcement orientation for the low-intensity treatment in both techniques is identical and does not change from that of the background material (in the centre). A small change is observed only after high-intensity treatment. Therefore, in Ti-base alloy the plasticity induced deformations are small to produce substantial work hardening.

The situation is different for Ni-base alloy: the reinforcement direction deflects even at low-intensity treatment; further deviation from the background reference orientation is observed as the treatment progresses. This is an indication of higher stiffness variation and more effective work hardening in Ni-base alloy.

In friction stir welds (FSW), a severe plastic deformation of the softened material is facilitated by the friction heat induced by the rotating welding tool. Both factors are supposed to be sensitive to the plunge depth of the tool, so that any variation of the plunging depth (that produces the lack-of-penetration (LOP)) modifies the plastic deformation pattern in the weld line.

An example of ultrasonic birefringence applied to NDT of LOP in the FSW line between 5mm thick aluminum plates is shown in Fig. 6. The area of the LOP defect occupied a part (45 – 100 cm) of the tool traverse distance (Fig. 6, left, bottom). The orientation of in-plane reinforcement was measured along the weld line and compared with that outside the weld.

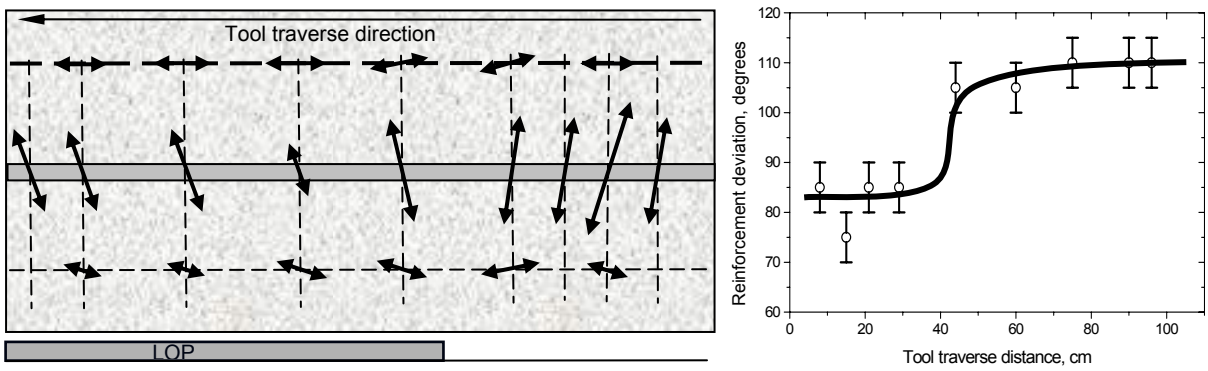

Fig. 6. Reinforcement pattern around FSW line (left, centre) with partial LOP defect (left, bottom). Axial deviation of reinforcement as a function of tool traverse distance (right); LOP area – (45 - 100) cm.

The reinforcement outside the weld is rather weak and basically aligned horizontally. In the FSW line (Fig. 6, left, centre), it enhances substantially and the orientation deviates strongly from the axial direction due to systematic material transfer by the rotating tool. As expected, the orientation of reinforcement changes as the tool enters into the LOP area. The step-wise variation of the deviation angle in Fig. 6, right is about 30 degrees which is quite sufficient for reliable NDT of the LOP defects.

3. NDT of stiffness anisotropy via air-coupled ultrasound

3.1. Depth-resolved probing of stiffness anisotropy

The slanted configurations of air-coupled ultrasound (ACU) are based on resonance mode conversion at an angle of incidence corresponding to plate (or surface) wave excitation in the specimen [3]. This methodology combines the benefits of a non-contact excitation of guided waves with a high spatial resolution and allows for remote NDT of in-plane anisotropy by measuring the wave velocity as a function of azimuth angle.

In multi-ply composite laminates, the guided wave velocity is determined by the contributions of all plies into an overall stiffness. However, if the particle motion caused by the wave is inhomogeneous over the plate thickness, each contribution will depend on the degree of "activation" for particular ply. A typical displacement pattern calculated for a flexural wave in a thin plate [4] (a_0-mode) is shown in Fig. 7. The out-of-plane component (W_{a_0}) is dominating but is basically homogeneous across the plate thickness (D). The in-plane displacement (U_{a_0}) is maximum on the plate surface and zero in the middle plane. As a result, maximum contribution to bending stiffness for a flexural wave is expected from the surface plies while the role of the middle plies is diminished.

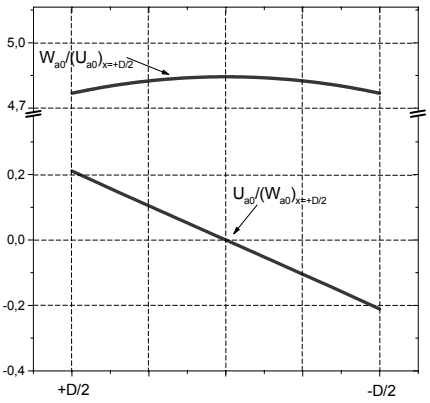

Fig. 7. Normalized in-plane and out-of-plane displacements in flexural mode.

To demonstrate the feasibility of the depth-resolved probing of stiffness, two specimens of unidirectional carbon fibre/epoxy (CFRP) prepregs (HexPly M18/1 G947 UD) were manufactured. The laminate plies [0/45/-45/90]s and [0/60/-60]s were made in a quasi-isotropic symmetrical lay-up in regard to the middle plane, which is common for most applications to avoid out-of-plane bending under plane stress conditions.

The results of birefringence measurements in transmission mode for the two specimens are shown in Fig. 8. Both the amplitude and phase curves are in close agreement with theoretical approach of section 2.1 (formulas (8) and (9) for $\Delta\varphi \approx 0$) and thus confirm the quasi-isotropic lay-up expected if the stiffness is averaged over the thickness of the samples.

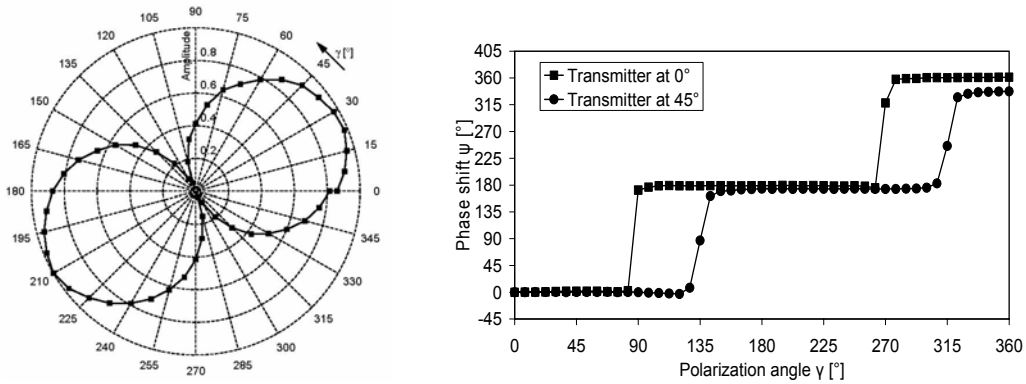

Fig. 8. Amplitude (left) and phase shift (right) of birefringence output signal as functions of receiver orientation for [0/60/-60]s (left) and [0/45/-45/90]s lay-ups.

As was shown above, unlike the bulk wave case the weighted averaging with the emphasis on the outer plies is expected for the flexural wave propagation. To generate and detect the flexural waves in CFRP laminates 200 kHz ACU transducers were used in a single-sided access configuration [5]. The phase of the received signal as a function of distance between the transducers was measured for precise evaluation of flexural wave velocity. Owing to non-contact excitation/detection, the change in the propagation direction (α) was readily managed by rotation of the specimens in azimuth plane.

The measurement results (Fig. 9) reveal a noticeable velocity anisotropy in the laminates. In both cases the maximum velocity is obtained for propagation along the outer 0^0 –plies. The in-plane velocity anisotropy is 12% in the [0/45/-45/90]s and 14% in the [0/60/-60]s laminate. The minimum velocity is shifted from the orthogonal direction due to the influence of the remaining ply lay-up. This effect is seen in Fig. 9, right for the [0/60/-60]s laminate where the flexural wave velocities in the first/third quadrants appear to be higher than those in the second/fourth quadrants. The difference is caused by a greater contribution to the stiffness by the subsurface plies $+60^0$ than that by -60^0 layers which are closer to the middle plane.

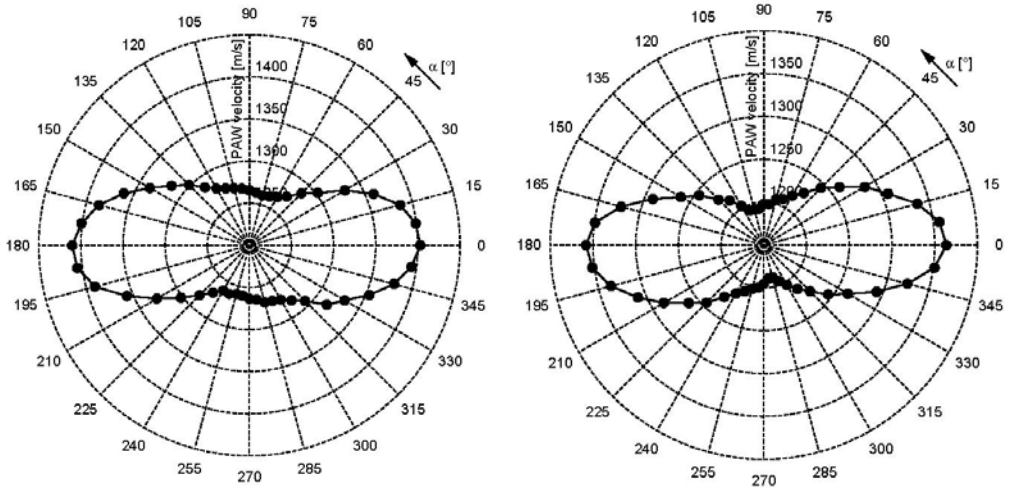

Fig. 9. Flexural wave velocity anisotropy in [0/45/-45/90]s (left) and [0/60/-60]s (right) CFRP laminates.

3.2. Frequency dependence of flexural wave velocity anisotropy

The results of the previous section show that the flexural wave anisotropy is depth-selective and thus depends on the order of dissimilar plies comprising the laminate. However, even for identical orientation of plies in a lay-up the in-plane anisotropy is not constant but a function of frequency.

This effect was studied for a quasi-unidirectional laminate of 20-ply high-strength CFRP (size 34x24x0.25 cm^3, weight fibre content $\approx$50%) consisting of (2x9) unidirectional (0^0) carbon fibre plies and 2 fabric carbon fibre ($\pm 45^0$) plies in the middle.

The focused slanted transmission mode (FSTM) of air-coupled ultrasound [3] was applied for remote probing of the flexural wave velocity anisotropy. The technique is based on the measurements of the angle of incidence (θ) corresponding to resonance ACU transmission: $\sin\theta = v_{air} / v_{a_0}$. The FSTM measurements were implemented along (0^0) and across (90^0) fibre direction with 50 kHz-air-coupled transducers (the Ultran Group). The bandwidth of the transducers was broad enough to observe signal transmission in $f = (40 - 100)$ kHz frequency range. The duration of the input bursts of maximal 300V-amplitude was increased to 20 cycles of carrier frequency to provide the excitation close to monochromatic.

To further extend the operation frequency range a wide-band contact piezo-transducer was attached in the central area of the specimen; a continuous wave input signal of ~50 V amplitude provided efficient excitation of cylindrical a_0-wave over the frequency range up to 250 kHz. A Doppler scanning laser vibrometer (Polytec) was used for animated wave form imaging (WIM) (Fig. 10). The plot function of the laser vibrometer (Fig. 10, bottom) enabled precise measuring of the wavelength and phase velocity estimation for 0^0 and 90^0 directions.

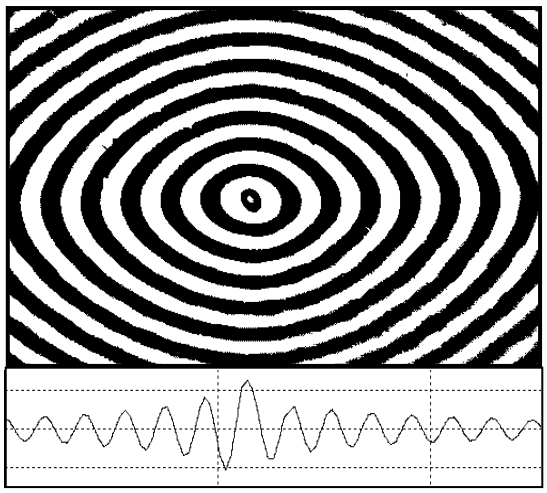

Fig. 10. 70 kHz cylindrical flexural waveform in unidirectional CFRP.

The FSTM measurements were made for each 10 kHz-step in the range (10 – 40) kHz; the WIM velocity measurements were extended up to 250 kHz with a larger frequency step. The experimental results are summarized in Fig. 11 which shows the dispersion curves of a_0-modes for 0^0- and 90^0-propagation directions. The dispersion curves obtained are typical for the a_0-modes in both isotropic and anisotropic materials with phase velocity increase from zero to asymptotic value of the surface acoustic wave (SAW) velocity at high frequencies.

The anisotropy of velocity can be characterized by introducing the parameter of anisotropy as the ratio of the phase velocities along 0^0- and 90^0-directions: $A = v^0 / v^{90}$. From the data in Fig. 11, the frequency variation of the anisotropy parameter for the a_0-modes is calculated and presented in Fig. 12. Maximum anisotropy corresponds to $f \to 0$; as the frequency increases, it exhibits a sharp descent from a certain "static" value to an asymptotic plateau at higher frequencies.

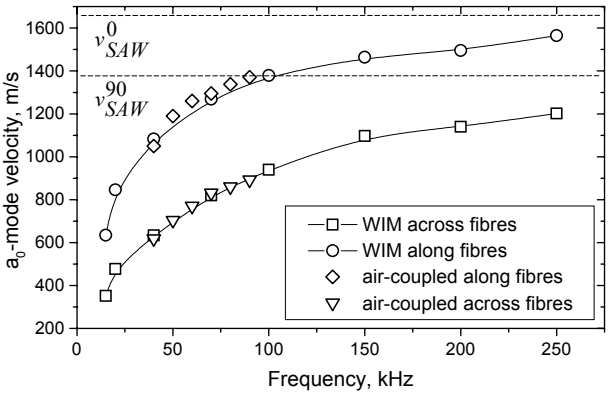

Fig. 11. Dispersion of a_0-waves in CFRP measured with WIM and ACU; dotted lines are high-frequency asymptotes for principal direction.

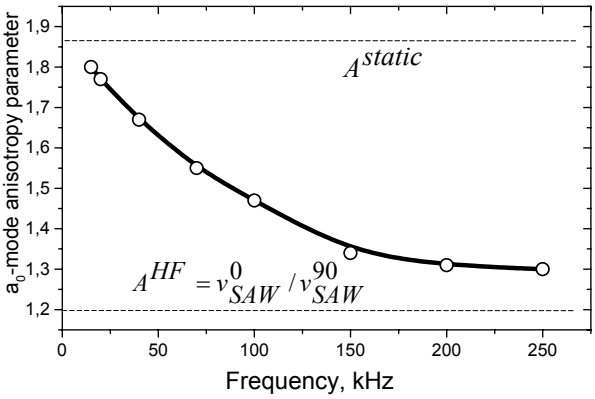

Fig. 12. Frequency dispersion of anisotropy for a_0-waves in CFRP; dotted lines are estimates for asymptotic behaviour.

The frequency behaviour of flexural wave anisotropy can be interpreted on the basis of the dispersion relation for a_0-modes valid for $f \to 0$:

$$v_{a0} \approx (\pi D f v_{s0} / \sqrt{3})^{1/2} \quad , \tag{9}$$

where v_{s0} is the low-frequency (dispersion free) velocity of zero-order symmetrical wave.

The low-frequency value of anisotropy parameter then takes the form: $A^{static} = (v^0_{s0} / v^{90}_{s0})^{1/2}$.

The s_0-modes exhibit predominantly in-plane polarization over the dispersion-free frequency range that makes the air-coupled excitation inefficient. A simplified approach to evaluation of v_{s_0} in ACU experiments was developed by Luukkala for isotropic materials [6] (and also applicable to orthotropic plates [7]). It takes into account that $v_{a_0} = v_{air} / \sin\theta$ in (9), so that v_{s_0} can be found by measuring frequency dependence of the excitation angle θ:

$$v_{s_0} \lim_{f \to 0}(f \sin^2\theta) = v_{air}^2 \sqrt{3} / \pi D \quad . \tag{10}$$

The application of this approach is demonstrated in Fig.13. The linear extrapolation of the experimental data (for propagation angles 0^0, 45^0 and 90^0) to the low-frequency range is used to obtain the left-hand side limit in (10). The values of v_{s_0} derived from (10) are given in Table 1 and used to estimate the value of the anisotropy parameter: $A^{static} \cong 1.87 \pm 0.04$. This value fits readily to the low-frequency extrapolation of the experimental results (Fig. 12). A physical reason for maximum anisotropy in the static case is concerned with maximum contribution of tensile deformation to bending stiffness.

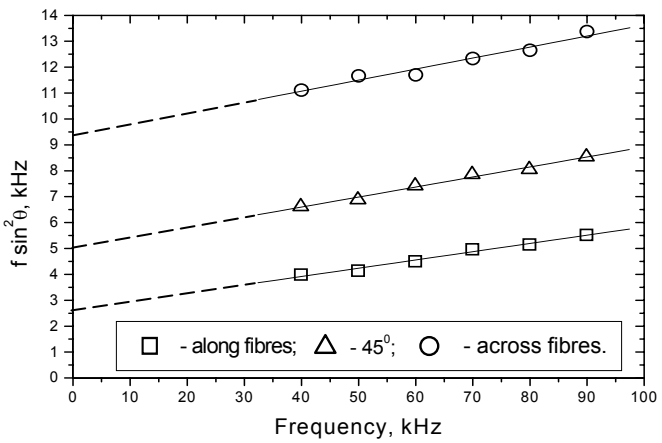

Fig.13. Low-frequency extrapolation of air-coupled measurements of a_0-wave velocities.

At high frequencies, the a_0-modes are gradually converted into surface waves which determine the high-frequency end of the anisotropy dispersion curve in Fig. 12. The SAWs are non-dispersive; they produce mainly shear out-of-plane near-surface deformation and are expected to have lower elastic anisotropy. This was confirmed by the SAW velocity measurements in the axial directions of an 80-ply unidirectional CFRP lay-up (thickness 10.5 mm). The edge-bonded transversal wave transducers [8] were used to generate and detect the SAWs. The measured SAW velocity values given in Table 1 and presented in Fig. 11 yield the high-frequency limit for the anisotropy parameter:

$$A^{HF} = (v_{SAW}^0 / v_{SAW}^{90}) \cong 1.2 \pm 0.3, \tag{11}$$

that indicates a reasonable asymptotic behaviour of the frequency dependent anisotropy in Fig. 12.

Table 1. Guided wave velocities in CFRP.

Velocity	Propagation direction	Value (m/s)
$v_{s_0}^{ACU}$	X_1 (0^0)	9600 ± 1000
$v_{s_0}^{ACU}$	X_2 (90^0)	2700 ± 300
v_{SAW}	X_1 (0^0)	1680 ± 30
v_{SAW}	X_2 (90^0)	1380 ± 20

Conclusions

The parameters of elliptical motion induced by birefringent shear waves provide information on stiffness anisotropy which can be caused by internal stresses, texture, molecular or/and fibre orientation. On this basis, a simple experimental technique which uses standard ultrasonic NDT equipment is developed and applied for mapping of fibre orientation in composite materials. It is also shown to work reliably in determining the reinforcement induced by cold work and defects of a lack-of-penetration in friction stir welds in metals and alloys. Additional experiments proved that the technique is sensitive to detect damage induced variation in stiffness anisotropy and is applicable to a number of fibre-reinforced materials including single- and multi-ply lay-ups, non-fabric and multi-ply fabric composites.

In bulk wave NDT, the ultrasonic data are always averaged over the volume of the specimen so that depth-dependent features of the materials (in particular, multi-ply composites) are ignored. The depth-resolved NDT of stiffness is feasible by using guided ultrasonic waves and flexural waves in particular. The particle motion induced by flexural modes oscillates with depth and activates selected plies of the laminates. For zero-order waves, a contribution of outer plies into bending stiffness dominates. As a result, substantial in-plane velocity anisotropy induced by the surface plies manifests in CFRP specimens with quasi-isotropic lay-ups. The use of the higher-order modes of plate waves will make possible to single out the contribution of other internal plies and make an overall conclusion on the structure of multi-ply laminate.

In ultrasonic frequency range, the velocity anisotropy measured by using the bulk wave is independent of frequency and fully determined by elastic moduli of material. In plate-like anisotropic materials, the velocity in-plane anisotropy is not constant but a function of frequency even for materials deemed to be homogeneous and non-dissipative. The reason for that is concerned with velocity dispersion which affects the wave propagation in different ways for various azimuth directions and thus modifies the elastic anisotropy pattern. Such an effect of dispersion of elastic anisotropy is of importance in dynamic testing and elastic wave applications of anisotropic materials.

Acknowledgement

The financial support of the German Research Foundation (DFG) in the framework of the project Bu 624/26-2 is gratefully acknowledged.

References

1. B.A. Auld, A*coustic Fields and Waves in Solids,* v. 1, John Wiley & Sons: New York, 1973.
2. Igor Solodov, Klaus Pfleiderer, Daniel Döring, and Gerd Busse, NDE of anisotropy in composite materials via acoustic birefringence, Research in NDE, v. 19, pp. 129 -143, 2008.
3. I. Solodov, R. Stoessel, G. Busse, Material characterization and NDE using focused slanted transmission mode of air-coupled ultrasound, Research in Non-Destructive Evaluation, v.15, pp. 1-21, 2004.
4. A. Krug, Air-coupled Lamb waves for thickness measurements, Diploma thesis, University of Stuttgart, 2005.
5. D. Döring, I. Solodov, and G. Busse, Air-coupled surface acoustic waves: opportunities and limitations for NDT application. Proc. 4th Workshop NDT in Progress, Prague, pp. 51 – 62, 2007.
6. M. Luukkala, P. Heikkila, J. Surakka, Plate wave resonance – a contactless test method, Ultrasonics, pp. 201- 208, 1971.
7. C.C. Haberger, R.W. Mann, and G.A. Baum, Ultrasonic plate waves in paper, Ultrasonics, pp. 57–62, 1979.
8. I.A. Viktorov, *Rayleigh and Lamb Waves*, Plenum Press, New York, 1967.